ARMA 19–254

Variation of the least principal stress with depth and its effect on vertical hydraulic fracture propagation during multi-stage hydraulic fracturing

Xu, S., Singh, A., and Zoback, M.D.
Stanford University, Stanford, CA, USA

This paper was prepared for presentation at the 53rd US Rock Mechanics/Geomechanics Symposium held in New York, NY, USA, 23–26 June 2019. This paper was selected for presentation at the symposium by an ARMA Technical Program Committee based on a technical and critical review of the paper by a minimum of two technical reviewers. The material, as presented, does not necessarily reflect any position of ARMA, its officers, or members. Electronic reproduction, distribution, or storage of any part of this paper for commercial purposes without the written consent of ARMA is prohibited. Permission to reproduce in print is restricted to an abstract of not more than 200 words; illustrations may not be copied. The abstract must contain conspicuous acknowledgement of where and by whom the paper was presented.

ABSTRACT: Knowledge of the least principal stress within, above and below producing intervals is essential for determining fracturing procedures that limit vertical propagation of hydraulic fractures to the intended range of depths. To better understand the cause of varying stress magnitudes in formations adjacent to unconventional reservoirs, we have combined laboratory studies of viscoplastic creep with numerical modeling utilizing in an attempt to match a profile of least principal stress measurement with depth in an actual case study. Creep experiments were conducted on core samples from different depths of a shale play in which Diagnostic Fracture Injection Tests (DFITs) were performed to determine the least principal stress. A power law creep model was used to fit the experimental data. The least principal stress was calculated from numerical modeling with a power law creep law using Abaqus. The calculated least principal stresses were found able to match the relative change of the observed stress magnitudes indicating that the variation of the least principal stress is controlled by varying amounts of viscoplastic stress relaxation. We demonstrate how the observed variations of the least principal stress with depth have an important influence on vertical hydraulic fracture propagation.

1. INTRODUCTION

A number of case studies have shown that the magnitude of the least principal stress can vary from layer to layer in unconventional oil and gas plays. Because such stress variations can have an important impact on vertical hydraulic fracture growth, we investigate here one physical mechanism that could be responsible for such stress variations. For the past several years, researchers in our research group have investigated the possibility that varying degrees of viscoplastic stress relaxation can lead to subtle, but important, variations of stress magnitudes in a sedimentary sequence (*e.g.,* Sone and Zoback, 2014b). Another way of saying this is that the more ductile a formation is, the more isotropic the stress magnitudes will become. In most areas this results in higher values of the least principal stress, i.e. higher frac gradients (Xu et al., 2017). Previous studies show that both clay-rich unconventional reservoir rocks (Sone and Zoback, 2014a) and carbonate-rich unconventional reservoir rocks (Rassouli and Zoback, 2018) exhibit time-dependent creep under constant axial load.

In this study, creep experiments were run, typically for one day, with a confining pressure and axial load similar to in situ conditions to characterize the ductile properties of core samples.

The core samples used in the laboratory testing came from a vertical well in which a profile of least principal stress measurements were made using DFIT tests at approximately the same depths. In the six layers shown in Fig. 1, the least principal stress varies between 69 MPa and 80 MPa. The least principal stress in layer D (the pay zone in which the horizontal wells are drilled) is 76 MPa. It is slightly higher in layers E and F below layer D, but lower in formations A, B, and C in shallower formations. The DFIT tests are shown in Appendix A.

One-dimensional creep constitutive parameters were determined from the laboratory tests using a relatively simple 1-D analytical creep law following (Sone and Zoback, 2014a). Subsequently, Abaqus was used to simulate the creep of the one-inch core samples and how it would affect stress relaxation in situ. We then developed a crustal loading model in Abaqus to estimate stress magnitudes in 5 of the 6 layers. Finally, we utilized the vertical profile of least principal stress to simulate hydraulic fracture propagation and proppant placement using ResFrac (McClure and Kang, 2018).

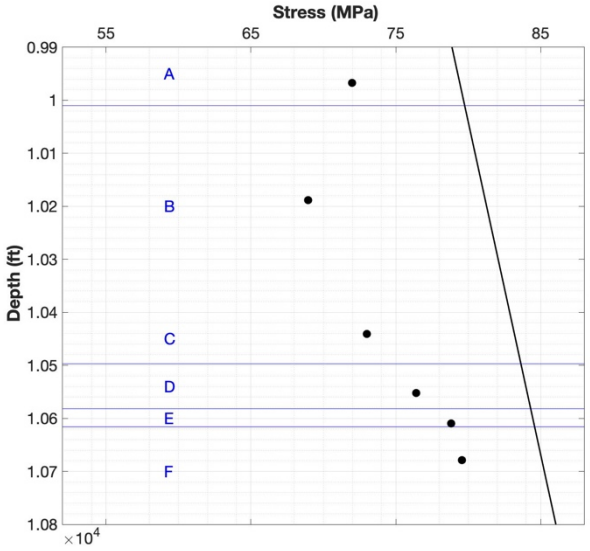

Fig. 1. The least principal stress determined from DFITs at six different depths where core samples are also available for laboratory testing.

2. METHODS

2.1. Laboratory Creep Experiments

The samples we used are horizontal sidewall plugs cored from the six formations. They are 0.851 inches to 1.495 inches long and 1 inch in diameter. Mineral compositions of core samples in the same well and close to the depths of samples conducted creep experiments are shown in Table 1. The samples vary from clay-rich to carbonate-rich.

Table 1. Mineral compositions of nearby samples

Sample formation	Depth (ft)	Carbonate (%)	QFP (%)	Clay (%)	TOC (%)
A	9946.5	23.5	27.8	48.6	0.1
B	10185.6	16.9	25.6	57.2	0.3
C	10438.5	18.4	28.1	52.9	0.6
D	10539.0	44.2	26.1	26.2	3.5
E	10607.4	57.8	14.9	25.0	2.3
F	10675.1	82.6	14.4	2.9	0.1

The equipment used is a high pressure triaxial rock mechanics system (GCTS) shown in the upper left of Fig. 2. Strain of the samples is measured by either LVDTs (as shown in the upper right of Fig. 2) or strain gauges (as the shown in the lower left of Fig.2). LVDTs can measure the strain to an accuracy of 10^{-6}, while strain gauges can measure the strain to an accuracy of 10^{-7}. The range of strain gauge measurement can be as large as 5%. The advantage of using strain gauges versus LVDTs is that the lateral strains can be more accurately measured. The jacketed sample is show in the lower right of Fig. 2.

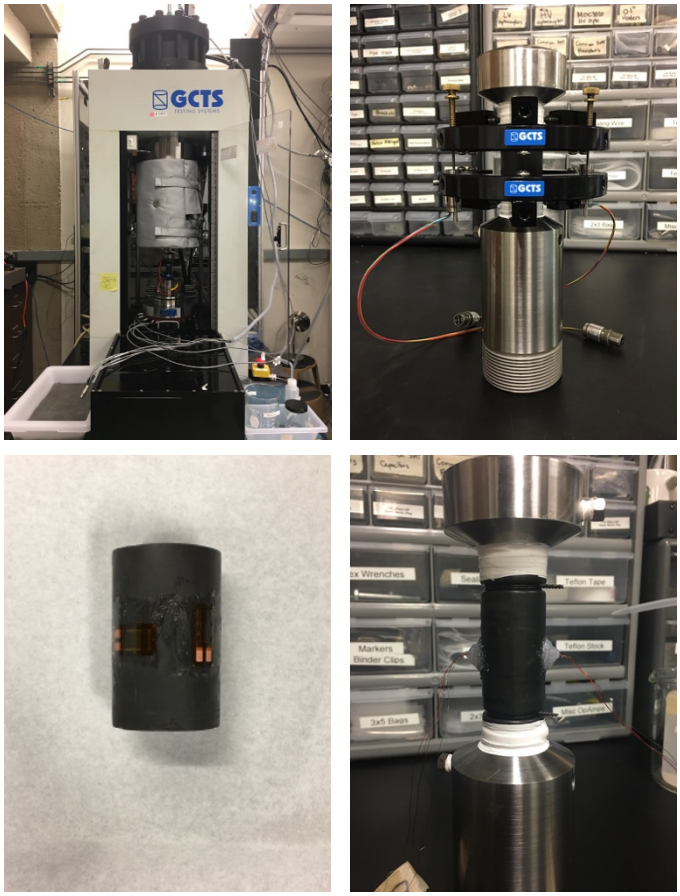

Fig. 2. Geological Consulting and Testing System (GCTS) with a core sample between two core holders installed on (upper left); A core sample set up with LVDTs (upper right); Axial and lateral strain gauges attached on a shale sample (lower left); A jacketed core sample with sealing wires on and strain gauges wires going through and sealed (lower right)

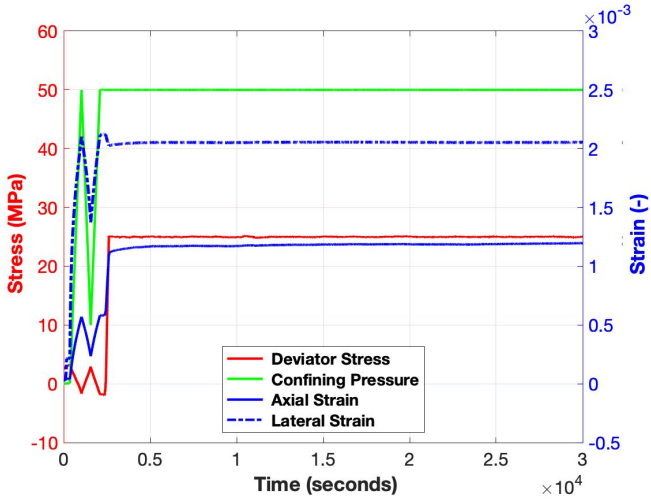

Fig. 3. One-day creep experiment raw data (deviator stress, confining pressure, axial strain, and lateral strain).

Above in Fig. 3 are the raw data of a one-day creep experiment of the formation C sample. The confining pressure is added to 0.1 MPa at first, followed by increasing the confining pressure 4.5 MPa per minute to 50 MPa. The confining pressure is then decreased to 10 MPa in the same rate and increased to 50 MPa again as a seasoning procedure for the sample. As both the axial and the lateral strains are measured during seasoning, we can obtain the bulk modulus. The axial piston is pushed up during this period which leads to a 2 MPa negative deviator stress. And this serves as the starting point of calculating differential stress. After the axial piston contacts the core holder, which can be seen from the axial load and the strain gauge signals, the deviator stress is increased 1 MPa every 8 seconds to 25 MPa. A sudden axial load is not chosen to be applied as instantaneously applying axial load easily breaks the rock. As the time of elevating deviator stress is short, Young's modulus can be fitted from the axial stress versus the axial strain change by assuming the material is elastic and elastic superposition can be imposed. The lateral strain is also measured during this period, so that Poisson's ratio is able to be calculated from lateral strain change and axial strain change. After this, the sample is kept under 50 MPa confining pressure and 25 MPa deviator stress for one day. The creep strains of both the axial and lateral directions are measured, which is the 24-hour creep part of the data. It is worth noting that the formation E sample is only measured less than 3 hours and the confining pressure intensifier is accidentally stopped. As the creep data is short in time, the formation E sample is not used to calculate the least principal stress using Abaqus.

2.2. *One Dimensional Creep Model*

The one-dimensional power law proposed by Sone and Zoback (2014a) is:

$$\varepsilon(t) = \sigma_0 J(t) \tag{1}$$

$$J(t) = Bt^n \tag{2}$$

where σ_0 is the differential stress. *J(t)* is a compliance function equal to the axial strain $\varepsilon(t)$ per unit of differential stress σ_0. B is a constant measuring the elastic compliance of the rock. n is a dimensionless parameter that describes the tendency of the rock to exhibit time-dependent deformation. Substituting the compliance function *J(t)* of Eq. 2 in Eq. 1, the constitutive law essentially describes the axial strain of time is equal to the differential stress σ_0 times constant B times time to a power of n.

2.3. *Numerical Modeling with Abaqus*

Our model using Abaqus for a one-inch sample creep is shown in Fig. 4, which is an elastic-creep model. For the creep part, the power law is defined in a time hardening form of Eq. 3

$$\dot{\bar{\varepsilon}}^{cr} = B^{cr}\bar{\sigma}t^{n^{cr}-1} \tag{3}$$

$$\dot{\bar{\varepsilon}}^{cr} = \sqrt{\frac{1}{2}\left[\left(\dot{\varepsilon}_1^{cr} - \dot{\varepsilon}_2^{cr}\right)^2 + \left(\dot{\varepsilon}_2^{cr} - \dot{\varepsilon}_3^{cr}\right)^2 + \left(\dot{\varepsilon}_3^{cr} - \dot{\varepsilon}_1^{cr}\right)^2\right]} \tag{4}$$

$$\bar{\sigma} = \sqrt{\frac{1}{2}\left[\left(\sigma_1 - \sigma_2\right)^2 + \left(\sigma_2 - \sigma_3\right)^2 + \left(\sigma_3 - \sigma_1\right)^2\right]} \tag{5}$$

where $\dot{\bar{\varepsilon}}^{cr}$ is the equivalent creep strain rate, which is the second invariant of the strain rate tensor as Eq. 4. And $\bar{\sigma}$ is the equivalent stress, which is the second invariant of the stress tensor as Eq. 5. B^{cr} and n^{cr} are calculated using the creep strain of the experimental data, while B and n are fitted using the total strain after the axial piston contacts the core holder. An assumption of this three-dimensional creep constitutive law is that the volume of the creep part of the material does not change, in other words, this is a deviatoric creep constitutive law.

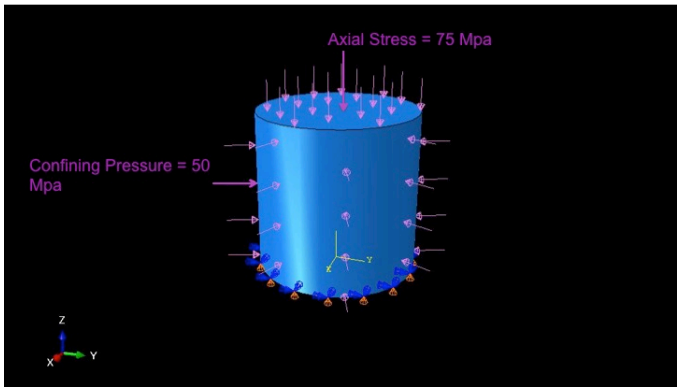

Fig. 4. Specified stress boundary conditions on a 1-inch long and 1-inch in diameter core sample in Abaqus

In the creep simulation, a 50 MPa confining pressure is specified first, and a 25 MPa differential stress is specified after the confining pressure. By specifying the stress boundary conditions this way, the numerical creep experiment is tried to be loaded as close to the laboratory conditions as possible. The differential stress is kept constant for one day to calculate the axial creep strain. Different B^{cr} and n^{cr} are experimented in the calculation, so that the axial creep strain is able to fit the experimental data for samples in different formations. The L_2 norm is used to calculate the similarity between numerical axial creep strain and the experimental data. The smallest L_2 norm is used to find the best fitted numerical creep strain. An example is shown in Appendix B-1.

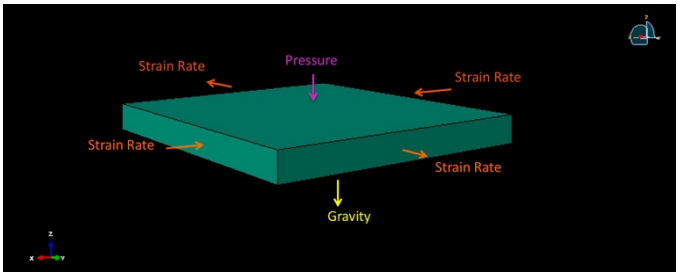

Fig. 5. Boundary conditions specified to calculate the evolution of the stress as a function of time in a specific formation

The boundary conditions of the stress relaxation simulation are specified as in Fig. 5. The bottom of the formation is constrained on the Z-direction. An overburden pressure equal to the overburden stress at a specific formation is specified on the top. As the sample is the sidewall plug and the studied well is in the strike-slip faulting environment, a compressive strain rate boundary condition is specified on the X-direction and an extensive strain rate boundary condition is specified on the Y-direction. The horizontal strain rate value is chosen as 4×10^{-13} / year, which is a typical number for intraplate strain rate (Tarayoun et al., 2018). A gravity is specified in the form of gradient which is calculated from density log. Under these boundary conditions, the least principal stress is able to be calculated as a function of time.

3. RESULTS

3.1. Viscoplastic Constitutive Parameters

Plotted in Fig. 6 is the differential stress and both axial and lateral strains data of the Formation C sample during elastic loading and creep after the contact of axial piston with the core holder. Both the axial and the lateral strains are the average of two strains measured on the opposite sides of the shale sample.

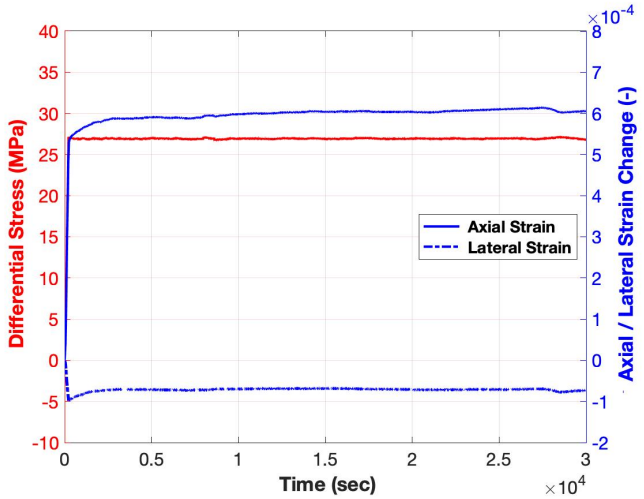

Fig. 6. Axial strain, lateral strain, and differential stress versus time

The red dash line in Fig. 7 is an example of fitting the experimental data using the one-dimensional power law described in section 2.2.

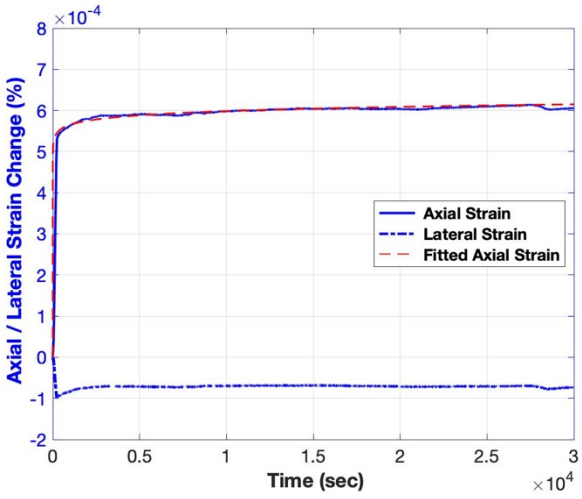

Fig. 7. Fitted axial strain using one dimensional power law creep model

Taking log of both sides of Eqn. 2 results in:

$$\log_{10}(J(t)) = \log_{10} B + n \log_{10} t \qquad (6)$$

where n and B are obtained from the slope and the intercept of the log-log plot as in Fig. 8. Plotting the axial strain data and highlight the creep part after 200 seconds by purple dots, the fitted curve is shown by the black dash line. The resolved constitutive parameters of six samples are shown in Table 2.

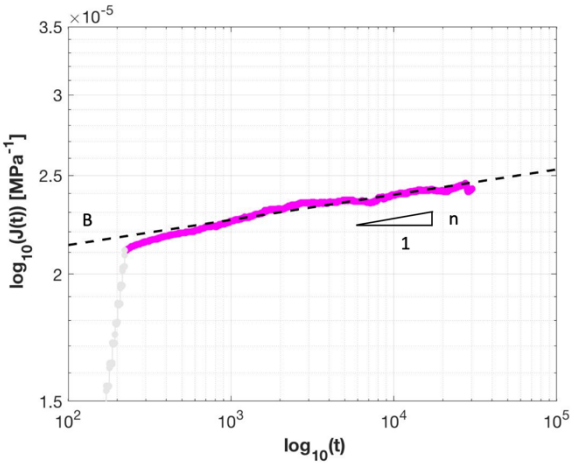

Fig. 8. Constitutive parameters of power law creep model fitted in a log-log base

Table 2. Resolved viscoplastic constitutive parameters from core samples at different formations

Sample formation	B (10^{-5} MPa^{-1})	n
A	2.0	0.039
B	1.6	0.021
C	2.0	0.024
D	2.2	0.037
E	3.2	0.021
F	1.7	0.031

B and n calculated from the one-dimensional model are listed in Table 2 for samples from six different depths. Comparing Table 2 and estimated least principal stress in Fig. 1, it is shown that for the formation with high least principal stress, either B or n is high, and for the formation with low least principal stress, both B and n are low. The larger the B and n, the more ductile the formation is. Therefore, the formation with larger degree of ductility leads to a more isotropic stress field, i.e. higher least principal stress.

3.2. Predicted Least Principal Stress

Following the creep constitutive parameters fitting and stress relaxation simulation described in section 2.3, we are able to resolve the constitutive parameters and calculate the least principal stress. For the upper three formations, 30000s of the experimental data are used, and the calculated least principal stresses are marked by open squares in Fig. 9; for formation D and formation F, as the late part of the experimental data are flat due to environmental factors, initial 12000s and 16000s of the data are used to fit the constitutive parameters, and the calculated least principal stresses are marked by solid triangles. An example of the fitted constitutive parameters from the axial creep strain after differential stress in Fig. 6 keeping constant for formation C sample is shown in Appendix B-1; and the calculated least principal stress as a function of time is shown in Appendix B-2.

Based on our calculations, the relative magnitudes of the least principal stress have positive correlation with the observed ones, implying the creep model is able to predict the least principal stress to the first order.

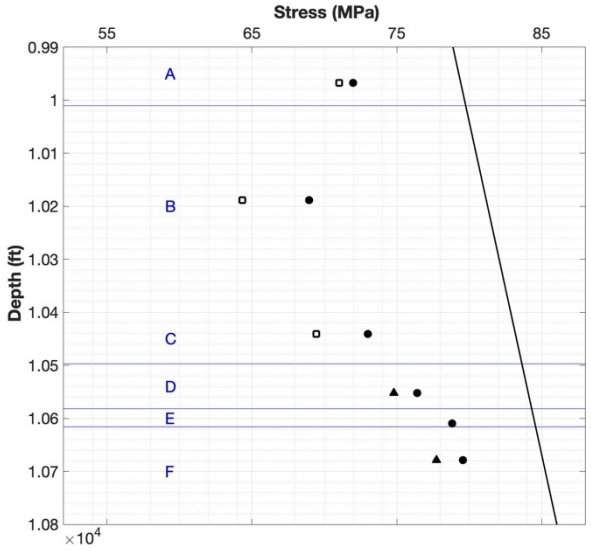

Fig. 9. Calculated least principal stresses based on Abaqus model using boundary conditions in Fig. 5 compare to measured values in Appendix A

4. DISCUSSION

The stress layering generated by different amount of stress relaxation in the lithological layers is a determining factor for hydraulic fracture footprint in response to fluid injection. The relative magnitudes of least principal stress determine not only the direction of hydraulic fracture propagation, but also the proppant distribution.

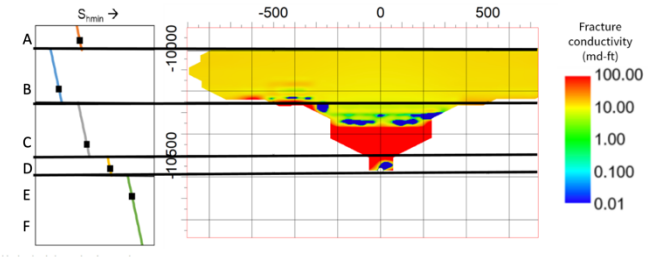

Fig. 10. The left panel shows the layered least principal stress configuration used for the modeling with the black squares indicating the stress measurements in formations A through E. The right panel shows the hydraulic fracture footprint after two weeks of shut-in, which indicates the upward hydraulic fracture growth driven by the vertical variations of least principal stress

We demonstrate this by modelling hydraulic fracture propagation for the upper 5 formations A, B, C, D and E with the stress profile shown in the left panel of Fig. 10. Formation F is not considered here for fracture propagation simulation. The black squares are the stress measurements from Fig. 1 with an assumed least principal

stress gradient in each layer. Assuming reasonable but homogenous rock properties, a simulation study has been done to illustrate the impact of hydraulic stimulation in formation D with the following operational parameters:

(i) Injection in formation D using slick water at 50 bbl/min for two and a half hours.
(ii) Single perforation cluster with a 0.32 inches perforation diameter and 12 perforations per cluster.
(iii) Proppant concentration of 1ppg with 40/70 mesh proppant.

The simulation study was done using ResFrac, with 3D coupled fracture propagation, matrix fluid flow and well-bore flow modelling capabilities. The simulator is described in detail by McClure and Kang, 2018. The right panel of Fig. 10 shows the footprint of the single hydraulic fracture after about two weeks of shut-in to give the proppant enough time to settle. The hydraulic fracture propagates upwards into the low least principal stress formations C and B with very little lateral propagation in formation D. Formations A and E act as stress barriers for the hydraulic fracture propagation. The color in the figure shows the fracture conductivity in the log scale with the red color indicative of the propped regions in the fracture. It is evident that the hydraulic fracture propagation and proppant placement are driven by the vertical variations of the least principal stress. This effect is discussed in detail in (Singh et al., 2019) for multiple hydraulic fractures propagating in close vicinity as would happen during a stage in plug-and-perf operations.

5. CONCLUSION

The magnitudes of least principal stress are affected by different degrees of viscoplasticity in different layers. The power law creep constitutive parameters are compared with the obtained least principal stress and it is found that the degree of viscoplasticity at different formations has positive correlation with the variations of least principal stress with depth. A numerical model is used to calculate the least principal stress as a function of time and the calculated least principal stress is found to be able to match the least principal stress measurements to the first order. The variations of the least principal stress with depth is demonstrated to be important to vertical hydraulic fracture propagation.

APPENDIX A

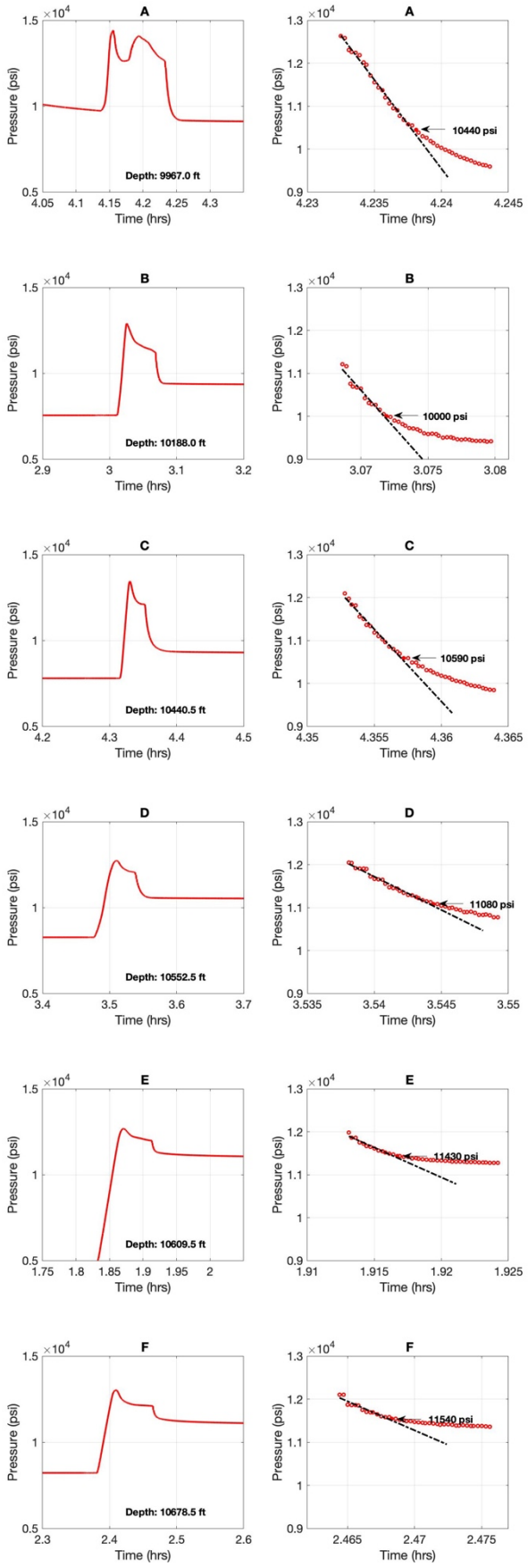

Fig. A. DFITs pressure versus time curves at the time window of injection and shut-in (left); ISIPs estimated from DFITs using a tangent method

APPENDIX B

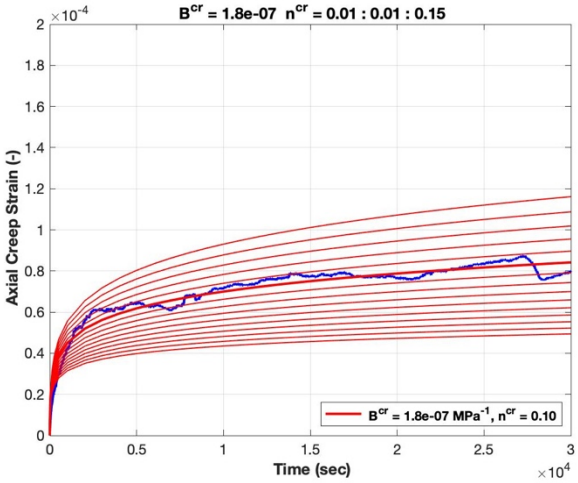

Fig. B-1. The numerical axial creep strain curves plotted over the experimental data with fitted constitutive parameters B^{cr} and n^{cr}

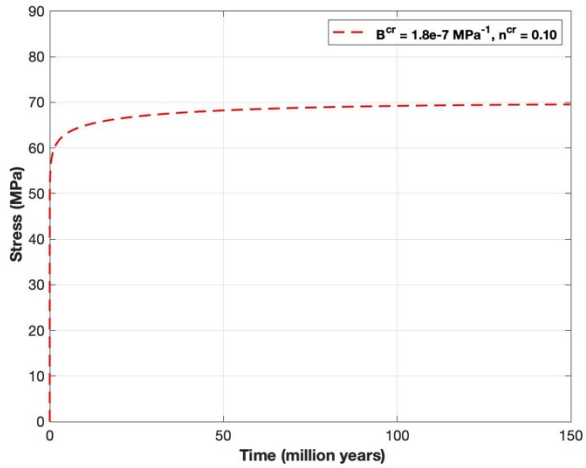

Fig. B-2. The calculated least principal stress using Abaqus with fitted B^{cr} and n^{cr} as a function of time

REFERENCES

1. Sone, H. and M.D. Zoback 2014a. Time-dependent deformation of shale gas reservoir rocks and its long-term effect on the in situ state of stress. *International Journal of Rock Mechanics and Mining Sciences*, Volume 69, Pages 120-132.
2. Xu, S., F.S. Rassouli, and M.D. Zoback 2017. Utilizing A Viscoplastic Stress Relaxation Model to Study Vertical Hydraulic Fracture Propagation in Permian Basin. *URTeC*, doi: 10.15530-urtec-2017-2669793
3. Sone, H. and M.D. Zoback 2014b. Viscous relaxation model for predicting least principal stress magnitudes in sedimentary rocks. Journal of Petroleum Science and Engineering, Volume 124, Pages 416-431
4. Rassouli, F.S. and M.D. Zoback 2018. Comparison of Short-Term and Long-Term Creep Experiments in Shales and Carbonates from Unconventional Gas Reservoirs. *Rock Mechanics and Rock Engineering*, Volume 51, Pages 1995-2014.
5. Evans, K. F., T. Engelder, and R. A. Plumb 1989. Appalachian Stress Study 1. A Detailed Description of In Situ Stress Variations in Devonian Shales of the Appalachian Plateau. *Journal of Geophysical Research: Solid Earth banner*, doi: 10.1029/JB094iB06p07129
6. Tarayoun, A., S. Mazzotti, M. Craymer, and J. Henton. 2018. Structural Inheritance Control on Intraplate Present-Day Deformation: GPS Strain Rate Variations in the Saint Lawrence Valley, Eastern Canada, *Journal of Geophysical Research: Solid Earth*, Volume 123, Pages 7004-7020.
7. McClure, M. and C. Kang. 2018. "ResFrac Technical Writeup," April. http://arxiv.org/abs/1804.02092.
8. Singh, A., S. Xu, M.D. Zoback, and M. McClure. 2019. Integrated Analysis of the Coupling Between Geomechanics and Operational Parameters to Optimize Hydraulic Fracture Propagation and Proppant Distribution. *Society of Petroleum Engineers*, doi:10.2118/194323-MS